Electrical Resistivity and Magnetoresistance in Monodispersed Oxide-Coated Fe Cluster Assemblies

Article *in* Japanese Journal of Applied Physics · February 2004

DOI: 10.1143/JJAP.43.674

3 authors, including:

Dong-Liang Peng
Xiamen University
179 PUBLICATIONS **2,083** CITATIONS
SEE PROFILE

T. Hihara
Nagoya Institute of Technology
201 PUBLICATIONS **1,687** CITATIONS
SEE PROFILE

Electrical Resistivity and Magnetoresistance in Monodispersed Oxide-Coated Fe Cluster Assemblies

2004 Jpn. J. Appl. Phys. 43 674

(http://iopscience.iop.org/1347-4065/43/2R/674)

Japanese Journal of Applied Physics
Vol. 43, No. 2, 2004, pp. 674–680

Electrical Resistivity and Magnetoresistance in Monodispersed Oxide-Coated Fe Cluster Assemblies

Dong-Liang PENG*, Takehiko HIHARA and Kenji SUMIYAMA

Department of Materials Science and Engineering, Nagoya Institute of Technology, Nagoya 466-8555, Japan

(Received July 22, 2003; accepted October 28, 2003; published February 10, 2004)

We systematically studied electrical resistivity and magnetoresistance (MR) of size-monodispersed oxide-coated Fe cluster assemblies with the mean cluster sizes of $d = 9$–17 nm prepared by a plasma-gas-condensation-type cluster beam deposition system. The electrical resistivity and magnetoresistance strongly depend on the temperature, surface oxidization degree of the clusters (namely O_2 gas flow ratio R_{O2}), Fe cluster size d, and magnetic field. The oxide-coated Fe cluster assemblies exhibit a large negative MR effect which is further enhanced at low temperatures due to the dominant contribution of the spin-dependent tunneling process between the Fe cores through the oxide shell layers. It has been found that the magnetic field dependence of the *MR* ratio at all temperatures shows no saturation tendency up to a maximum field $H = 50$ kOe and completely disagrees with the magnetization curves which indicate a saturation tendency. These results have been interpreted by consideration of the magnetic state of the Fe-oxide shell layers, spin-dependent tunneling mechanism, and intercluster magnetic correlation. The high-field nonsaturation behavior in the magnetoresistance effect is attributed to the spin-disordered structure, which is frozen in a spin-glass-like state at low temperatures, in the surface of the Fe-oxide shell crystallites or the whole thinner Fe-oxide shell layers. [DOI: 10.1143/JJAP.43.674]

KEYWORDS: cluster beam deposition, magnetoresistance effect, electrical resistivity, Fe/Fe-oxide cluster assembly, size monodispersivity, magnetic properties

1. Introduction

There has been a growing interest in obtaining various nanostructured materials by using different preparation methods and understanding their novel physical properties, which are significantly different from those of the corresponding bulk counterparts.[1)] Nanostructured magnetic materials are commonly characterized by the coexistence of magnetically and/or structurally different phases, which are modulated on a nanometer-length scale.[2–7)] It has been demonstrated extensively that the core-shell Co or Fe nanoparticles constituted by two different magnetic phases: the Co or Fe cores and the surrounding oxide layer, reveal the characteristic magnetic properties due to strong exchange coupling between the cores and shell layers.[8–16)] Such surface and interface effects, which strongly depend on the particle size, surface oxidization degree, and magnetic properties of the oxide shells (antiferromagnetism or ferrimagnetism), make an important contribution to the total particle anisotropy.[14,15)]

For the core-shell-type Co/CoO size-monodispersed cluster assemblies, we have reported the characteristic transport properties and enhanced tunnel-type magnetoresistance effect at low temperatures, arising from the uniform Co core size and CoO shell thickness.[17)] For the same core-shell-type Fe/Fe-oxide cluster assemblies, however, we found that the magnetoresistance behaviors are clearly different from that for the Co/CoO cluster assemblies. The magnetic field dependence of magnetoresistance exhibits no saturation tendency in fields up to 5 T even at low temperatures, which disagrees with magnetization curves. In this study, we focus our attention on electrical resistivity and magnetoresistance of the size-monodispersed oxide-coated Fe cluster assemblies. We study the correlations between the resistivity and magnetoresistance and the oxygen gas flow rate (namely surface oxidization degree) as well as initial Fe cluster size. We also discuss characteristic nonsaturation behavior on magnetic field dependence of magnetoresistance in the oxide-coated Fe cluster assemblies.

2. Experimental

The samples were prepared by the plasma-gas-condensation (PGC)-type cluster beam deposition apparatus, whose details have been described elsewhere.[18,19)] The PGC-type cluster beam deposition apparatus is mainly composed of three parts: a sputtering chamber, a cluster growth region and a deposition chamber. The vaporized atoms in the sputtering chamber are decelerated by collisions with a large amount of inert gas (pure Ar or Ar/He mixture with Ar gas flow rate: $R_{Ar} = 250$–500 sccm and He gas flow rate: $R_{He} = 550$ sccm) injected continuously into the sputtering chamber, and are swept into the cluster growth region, which is cooled by liquid nitrogen. The clusters formed in this region are ejected from a small nozzle by differential pumping and a central part of the cluster beam is intercepted by a skimmer, and then deposited onto a sample holder in the deposition chamber (10^{-5}–10^{-4} Torr). Using this system, we obtained size-monodispersed Fe clusters having the mean size of 7-17 nm and the standard deviation less than 10% of the mean size.[15)] For preparation of oxide-coated Fe cluster assemblies, we introduced oxygen gas through a nozzle set near the skimmer into the deposition chamber to form iron oxide shells covering the Fe clusters before deposition on the substrate. This process ensures that all Fe clusters are uniformly oxidized before the cluster assemblies are formed. The transmission electron microscopy (TEM) observation showed that all clusters are characterized with a strong contrast in their "core", but with a uniform gray contrast in their "shell". The electron diffraction (ED) pattern clearly indicated the coexistence of α-Fe phase and Fe_3O_4 or γ-Fe_2O_3 phase. It is not possible to differentiate between these two oxide phases by ED because their lattice parameters are very similar. The high-resolution transmission electron microscope image displayed that the oxide-coated Fe

*E-mail address: pengdl@mse.nitech.ac.jp

clusters were covered with Fe_3O_4 or γ-Fe_2O_3 shells composed of very small crystallites.[15] We used three kinds of substrates for the Fe cluster deposition: carbon-coated copper microgrids for TEM observation, polyimide films for magnetic measurement, and quartz substrates for conduction and magnetoresistance measurement. The effective film thickness of deposited clusters, t_e, was estimated using a quartz crystal thickness monitor, which measures the weight of the deposited clusters. Magnetic and magnetoresistance measurements were performed using a superconducting quantum interference device magnetometer between 5 and 300 K with the maximum field of 50 kOe. Electrical resistivity was measured using a conventional dc four-probe method, and *MR* measurement was made in fields applied parallel to the electrical current direction.

3. Results

Figure 1(a) shows the temperature (T) dependence of the electrical resistivity, ρ, for the oxide-coated Fe cluster assemblies with $d = 13$ nm prepared at $R_{O2} = 0$, 0.2, 0.5, 3 and 6 sccm. For $R_{O2} = 0$ sccm [see the inset of Fig. 1(a)], the sample exhibits ordinary metallic temperature dependence, characterized by the large residual resistance at low temperatures and a linear increase with increasing T at high temperatures. For $R_{O2} \geq 0.2$ sccm, the temperature coefficient of the resistivity (TCR) becomes negative. For the entire temperature range, the resistivity first increases with increasing R_{O2} and then becomes almost unchanged for $R_{O2} \geq 3$ sccm, probably because the oxidation is decelerated and reaches a stable state in the low O_2 pressure atmosphere ($< 6 \times 10^{-4}$ Torr). Moreover, the resistivity at low temperatures is 3–5 orders of magnitude larger than that at room temperature and about 5–7 orders of magnitude larger than that of the sample prepared at $R_{O2} = 0$ sccm. In addition, as T decreases, the ρ value monotonically increases as in the case of a semiconductor, while an abrupt increase at around 120 K corresponding to the Verwey transition temperature (T_v) of Fe_3O_4 bulk sample is not observed. This also suggests that the Fe-oxide shell layer is a nonstoichiometric Fe_3O_4 phase or a mixture of stoichiometric Fe_3O_4 and γ-Fe_2O_3 phases.

Figure 1(b) shows the temperature (T) dependence of high-field *MR* ratio, $[\rho_{H=50\,kOe} - \rho_0]/\rho_0$, for the oxide-coated Fe cluster assemblies with $d = 13$ nm prepared at $R_{O2} = 0$, 0.2, 0.5, 3 and 6 sccm, where magnetic field H was applied parallel to the current direction, and ρ_0 is the resistivity of the virgin sample in the zero field. For $R_{O2} = 0$ sccm [see the inset of Fig. 1(b)], we have observed a small positive magnetoresistance effect, similar to the case of the multilayers[20–22] and Pd–C granular films,[23–25] which has been ascribed to a weak localization effect. For $R_{O2} \geq 0.2$ sccm, a large negative magnetoresistance effect was observed. With decreasing T, the absolute value of *MR* monotonically increases and reaches to approximately 6% at $T = 20$ K for $R_{O2} = 6$ sccm.

Figures 2 shows $\log \rho$ vs $1/T$ curves for the oxide-coated

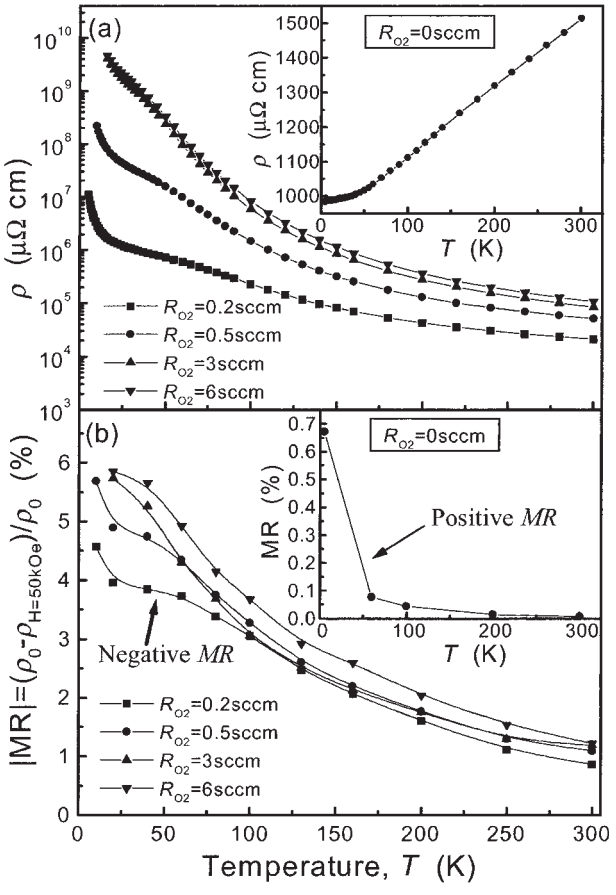

Fig. 1. Temperature dependence of (a) electrical resistivity ρ and (b) absolute value of the magnetoresistance ratio, $|MR|$, at $H = 50$ kOe for the oxide-coated Fe cluster assemblies with $d = 13$ nm prepared at $R_{O2} =$ 0, 0.2, 0.5, 3 and 6 sccm. The insets show the results for $R_{O2} = 0$ sccm.

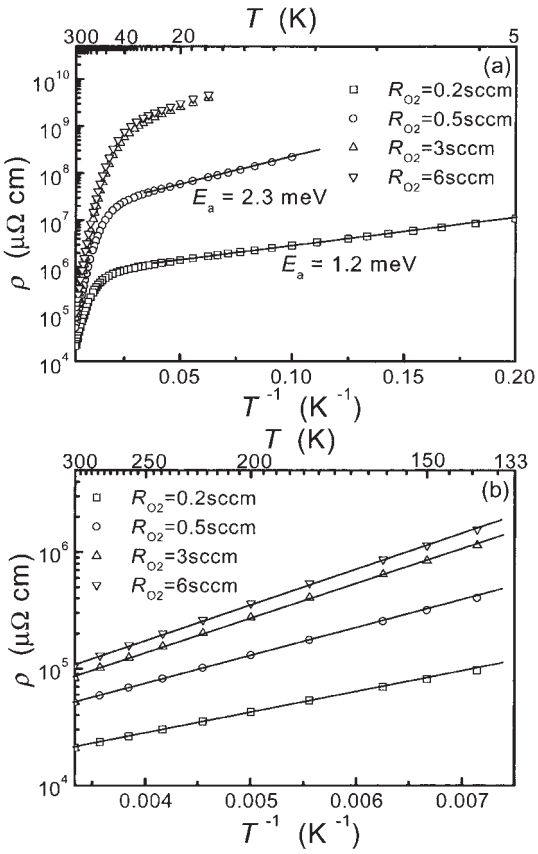

Fig. 2. Logarithmic resistivity, $\log \rho$, as a function of T^{-1} for the oxide-coated Fe cluster assemblies with $d = 13$ nm prepared at $R_{O2} = 0$, 0.2, 0.5, 3 and 6 sccm. Solid lines show the $\log \rho$ vs T^{-1} fitting.

Fe cluster assemblies with $d = 13$ nm prepared at $R_{O2} = 0.2$, 0.5, 3 and 6 sccm. As seen from Figs. 2(a) and 2(b), two linear dependences of $\log \rho$ on $1/T$ at low temperatures ($T < 30$ K for $R_{O2} = 0.2$ sccm) and at high temperatures ($T > 130$ K) were observed. Such a two-step-type linear temperature dependence of the resistivity was also observed in the size-monodispersed CoO-coated Co cluster assemblies obtained by the same preparation process.[17] It has been confirmed that the low-temperature linear $\log \rho$–$1/T$ relation originates from the tunnel-type conduction between Co cores through the CoO layers, and the uniform Co core size and CoO surface layer (barrier) thickness, while the high-temperature linear $\log \rho$–$1/T$ relation was believed to result from the polaron band-hopping conduction in the non-stoichiometric CoO semiconductor shell because there are usually a large number of defects and excess carriers in the transition metal oxides. The similar temperature dependence of the resistivity also indicates that similar mechanisms exist in the oxide-coated Fe and Co cluster assemblies. For the oxide-coated Fe cluster assemblies, the estimated activation energies (E_a) in the tunneling conduction temperature range ($T < 30$ K) are 1.2 and 2.3 meV for $R_{O2} = 0.2$ and 0.5 sccm. The E_a value should be related to charging energy E_c ($E_c = 2E_a$) which is the electrostatic energy required to create a positive-negative charged pair in two clusters by tunneling, and gives rise to the Coulomb blockade effect at very low temperatures.[17] E_c can be expressed as follows:[26] $E_c = (e^2/2\pi\varepsilon_0\varepsilon d_c)[s/(d/2+s)]$, where ε is the dielectric constant of the oxide shell layer, $\varepsilon_0 = 8.854 \times 10^{-12}$ F/m, d_c is the mean diameter of the metal cores and s is the separation between neighboring metal cores (namely the thickness of the oxide shell layer). Therefore, the E_a values estimated above are consistent with the expression of E_c: the oxide-coated Fe cluster assembly with a higher R_{O2} has a larger E_c value due to the decrease of Fe core size and the increase of Fe-oxide shell thickness with increasing R_{O2}. At $T > 130$ K [Fig. 2(b)], the estimated activation energies are 35, 47, 59 and 61 meV for $R_{O2} = 0.2$, 0.5, 3 and 6 sccm, respectively. These values also depend on R_{O2}, and increase with increasing R_{O2}, being attributable to defective or nonperfect structures of nonstoichiometric Fe-oxide semiconductor shell layers.

Figure 3 shows the temperature (T) dependence of (a) electrical resistivity, ρ, and (b) high-field MR ratio, $[\rho_{H=50\,kOe} - \rho_0]/\rho_0$, for the oxide-coated Fe cluster assemblies with $d = 9$, 13 and 17 nm prepared at $R_{O2} = 0.5$ sccm. Both ρ and MR increase with decreasing d. This result can be considered as interface and grain-boundary effects. With decreasing d, the number of grain boundaries and the volume of Fe-oxide shell layers in a unit length increase, and thus lead to the increase of ρ and MR.

Figures 4 shows $\log \rho$ vs $1/T$ curves for the oxide-coated Fe cluster assemblies with $d = 9$, 13 and 17 nm prepared at $R_{O2} = 0.5$ sccm. The estimated activation energies (E_a) in the tunneling conduction temperature range ($T < 30$ K) are 2.3 and 1.0 meV for $d = 13$ and 17 nm. Clearly, the estimated E_a values above are also consistent with the expression of E_c: the oxide-coated Fe cluster assembly with a smaller cluster size has a larger E_c value.

Figures 5 and 6 show the magnetic field dependence of MR ratio measured at 300, 100 and 60 K for the oxide-coated

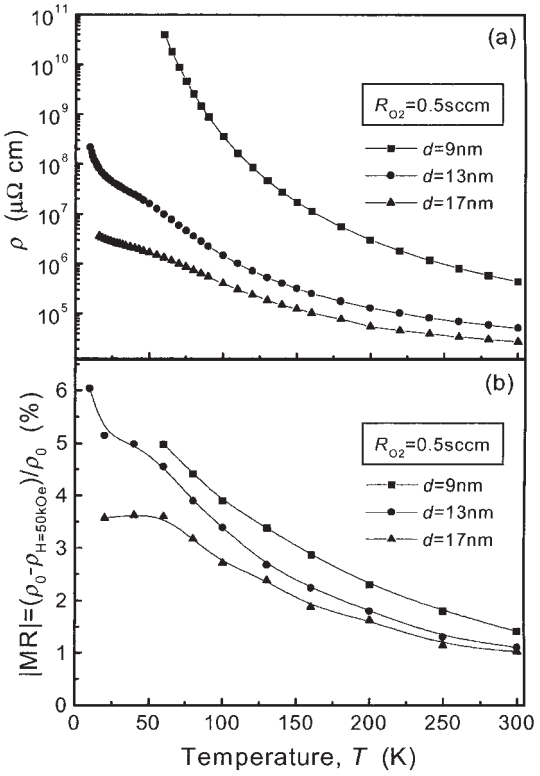

Fig. 3. Temperature dependence of (a) electrical resistivity ρ and (b) absolute value of the magnetoresistance ratio, $|MR|$, at $H = 50$ kOe for the oxide-coated Fe cluster assemblies with $d = 9$, 13 and 17 nm prepared at $R_{O2} = 0.5$ sccm.

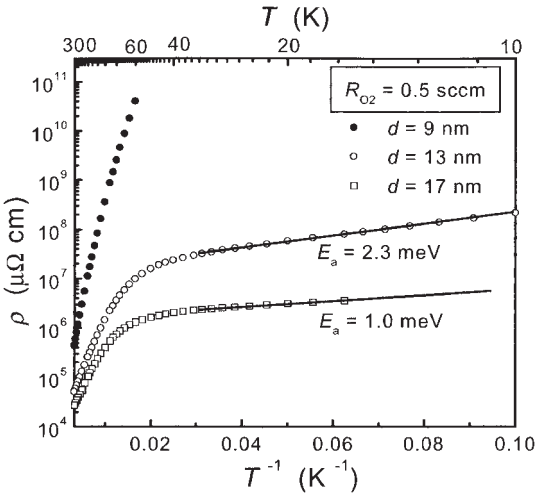

Fig. 4. Logarithmic resistivity, $\log \rho$, as a function of T^{-1} for the oxide-coated Fe cluster assemblies with $d = 9$, 13 and 17 nm prepared at $R_{O2} = 0.5$ sccm. Solid lines show the $\log \rho$ vs T^{-1} fitting.

Fe cluster assemblies with $d = 13$ nm prepared at $R_{O2} = 0.2$, 0.5, 3 and 6 sccm, and with $d = 9$, 13 and 17 nm prepared at $R_{O2} = 0.5$ sccm, respectively. As seen in Figs. 5 and 6, the magnetic field dependence of the MR ratio at all temperatures exhibits no saturation tendency up to $H = 50$ kOe. To further investigate the magnetic field dependence of MR ratio, we compared it with the magnetic field dependence of magnetization (Fig. 7). Clearly, the field-dependent feature of the MR effect [Fig. 7(b)] which exhibits no saturation tendency down to $T = 20$ K disagrees with the magnet-

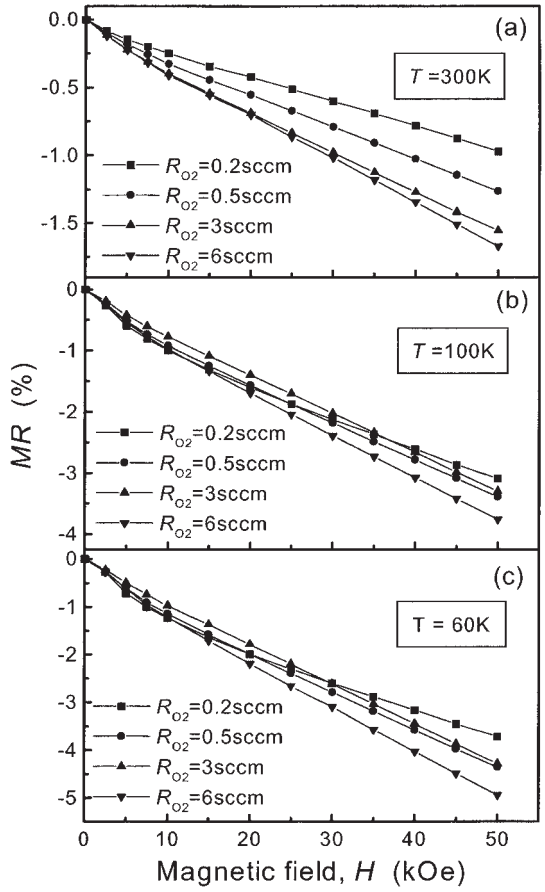

Fig. 5. Magnetic field dependence of *MR* ratio, $MR = (\rho_H - \rho_0)/\rho_0$, at different temperatures for the oxide-coated Fe cluster assemblies with $d = 13$ nm prepared at $R_{O2} = 0.2$, 0.5, 3 and 6 sccm.

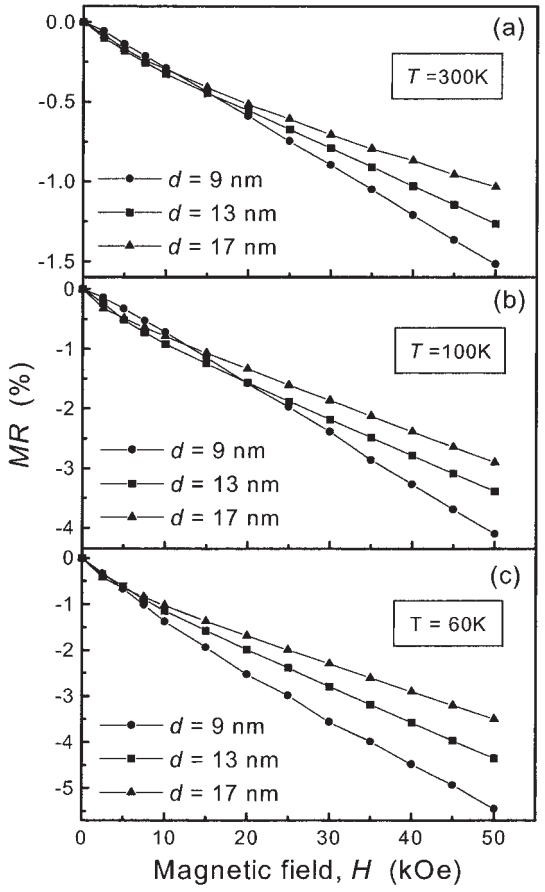

Fig. 6. Magnetic field dependence of *MR* ratio, $MR = (\rho_H - \rho_0)/\rho_0$, at different temperatures for the oxide-coated Fe cluster assemblies with $d = 9$, 13 and 17 nm prepared at $R_{O2} = 0.5$ sccm.

ization curves [Fig. 7(a)] which indicate a saturation tendency in spite of the gradual increase of magnetization for $H > 10$ kOe.

4. Discussion

Considering our surface oxidization process of the Fe clusters, and TEM and magnetic observation[15] for the oxide-coated Fe cluster-assembled materials, the Fe cluster cores are completely separated by the Fe-oxide shell layers whose thickness increases with increasing R_{O2}, although it cannot be quantitatively determined for different R_{O2} because we are not able to perform in situ TEM observation. In this case, there are mainly two conduction mechanisms: the thermal-activated-type conduction through the Fe-oxide semiconductor shell layers and tunnel-type conduction between Fe cores. As described in §3 (Figs. 1 and 3), at high temperatures ($T > 130$ K) the conductivity mainly results from the thermal-activated-type conduction through the network of the Fe-oxide shell layers, and at low temperatures ($T < 30$ K) from tunnel-type conduction between Fe cores because of the abrupt increase of the resistivity of the Fe-oxide shell layers with decreasing T, being similar to that observed in the size-monodispersed CoO-coated Co cluster assemblies.[17] However, the magnetic field dependence of the *MR* ratio at all temperatures shows no saturation tendency and disagrees with the magnetization curves, whereas for the CoO-coated Co cluster assemblies, it indicates a saturation behavior

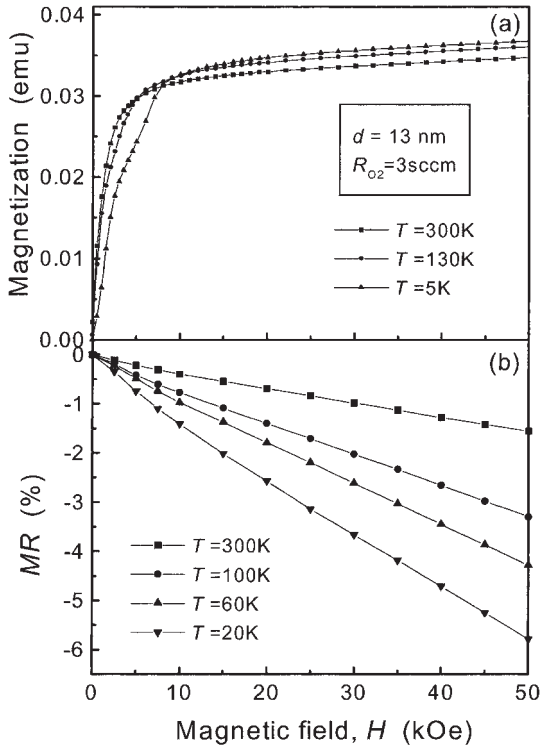

Fig. 7. Magnetic field dependence of (a) magnetization and (b) *MR* ratio, $MR = (\rho_H - \rho_0)/\rho_0$, at different temperatures for the oxide-coated Fe cluster assembly with $d = 13$ nm prepared at $R_{O2} = 3$ sccm.

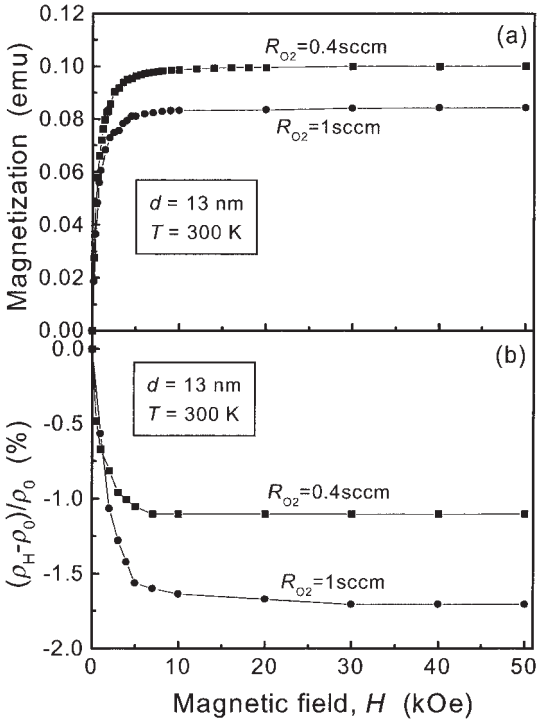

Fig. 8. Magnetic field dependence of (a) magnetization and (b) *MR* ratio, $MR = (\rho_H - \rho_0)/\rho_0$, at room temperature for the CoO-coated Co cluster assemblies with $d = 13$ nm prepared at $R_{O2} = 0.4$ and 1 sccm.

although it saturates more hardly at low temperatures than at high temperatures because of the exchange interaction between the ferromagnetic (FM) Co cores and the antiferromagnetic (AFM) CoO shells (the Neel temperature of bulk CoO is approximately 291 K). To further compare the difference between the oxide-coated Fe and Co cluster assemblies, we show the magnetic field dependence of magnetization and *MR* ratio measured at room temperature in magnetic field H applied parallel to the current direction for the oxide-coated Co cluster assemblies with $d = 13$ nm prepared at $R_{O2} = 0.4$ and 1 sccm (Fig. 8). As seen from this figure, the magnetic field dependence of the *MR* ratio [Fig. 8(b)] is well correlated with the magnetization curve [Fig. 8(a)] and exhibits a saturation behavior.

Let us now discuss the characteristic magnetoresistance behaviors and related mechanisms in the oxide-coated Fe cluster assemblies. In conventional FM–I granular systems where the magnetic metal granules or clusters are embedded in insulating matrices, the tunnel-type *MR* effect has also been detected[27] because the spin-dependent tunneling increases as the relative orientation of the magnetization (M) between granules or clusters gradually becomes parallel.[28] The transmission probability of the electrons across the insulating layer or nonmetallic layer is modified by the magnetic states of both metallic granules and nonmetallic layers (if magnetic). Moreover, for uncorrelated magnetic scatterers such as superparamagnetic magnetic granules,[29] the *MR* ratio should be proportional to M^2. Therefore, for the case of the CoO-coated Co cluster assemblies, a large *MR* effect results from a simple spin-dependent tunneling process between the FM Co cores through the CoO shell layer. It only depends on the relative orientation of the magnetizations of the cores because the Co-oxide (CoO) is AFM, being similar to the conventional FM–I granular materials and leading to the same magnetic field dependence in magnetization and *MR* (Fig. 8). For the present oxide-coated Fe cluster assemblies, however, the Fe-oxide (Fe_3O_4 or γ-Fe_2O_3) shell phase is ferrimagnetic (FIM), which is also different from the oxide-coated Co cluster assemblies. In this case, at low temperatures ($T \leq 100$ K), the *MR* effect depends not only on spin-dependent tunneling processes between the FM Fe cores through Fe-oxide shell layers but also on the magnetic state of FIM Fe-oxide shell crystallites, namely, the magnetic Fe-oxide shell layer strongly affects the transmission probability of the electrons across itself. Therefore, the magnetic state of the Fe-oxide shell layers plays an important role in determining the *MR* behaviors.

With regard to the magnetic states of the Fe-oxide shell layers, there are two interpretations: (1) superparamagnetic model above a blocking temperature of 30-40 K based on very small size of FIM Fe-oxide shell crystallites;[30] (2) the presence of spin disorder state, similar to spin glass, at and near the FM/FIM interface,[13,15] or in the whole Fe-oxide shells.[16] According to our systematic magnetic measurement results on the Fe-oxide-coated Fe cluster assemblies,[15] the superparamagnetic behavior of the FIM Fe-oxide shell crystallites cannot well explain the large training effect which is a diminution of exchange bias field (H_{eb}) upon the subsequent magnetization reversals. The decrease of H_{eb} is marked with increasing the training cycle number and H_{eb} is decreased to about 30% of the initial value after the 13th cycle. However, the second hypothesis mentioned above, namely spin-glass-like state, not only interprets all magnetic properties of the core-shell-type Fe/Fe-oxide clusters but was also supported by experimental observation. First, a Mossbauer spectroscopy study on surface oxidized Fe nanoparticles revealed that the surface shell consisted of small Fe-oxide crystallites have a large spin canting.[31–33] Second, thermal fluctuations of canted surface spins or a surface spin disorder in FIM nanoparticles[34–37] have been experimentally discussed, and found to freeze at low temperatures into a spin-glass-like phase with a multidegenerate ground state. The antiferromagnetic superexchange interaction is disrupted at the surface of the FIM oxide crystallites because of missing oxygen ions or the presence of other impurity molecules. Therefore, in the present oxide-coated Fe clusters, it is plausible that surface spins of the Fe-oxide shell crystallites (high R_{O2}) or spins of the whole thinner Fe-oxide shell layers (low R_{O2}) are canted or disordered because the oxide shells are thinner or the oxide shell crystallites are very small ($d < 2$ nm). The canted spins of the Fe-oxide shell layer could be frozen in a spin-glass-like state at low temperatures. Due to the presence of such a spin-glass-like state, even at low temperatures, the spin-dependent tunneling process of the electrons between the FM Fe cores is strongly affected by magnetic scatterers (spin-glass-like Fe-oxide shell layers), and thus the tunneling magnetoresistance (TMR) effect is also dominated by the Fe-oxide shell layers other than the FM Fe cores, giving rise to the nonsaturation tendency of the *MR* effect up to $H = 50$ kOe. In contrast, for the magnetization curves, the magnetization value mainly results from the FM Fe cores although there is an exchange interaction between the FM Fe cores and the Fe-oxide shell layers, and thus gives the

saturation tendency in spite of the gradual increase of magnetization for $H > 10$ kOe.

With increasing temperature, the origin of the *MR* effect becomes more complex because of the rapid decrease of the resistivity of the Fe-oxide shell layers. According to the temperature dependence of the resistivity in §3, at high temperatures ($T > 130$ K), the conductivity mainly results from the thermal-activated-type conduction in the Fe-oxide shell layers. In this case, the *MR* effect could be dominated by two spin-dependent tunneling processes between the FM Fe cores and the Fe-oxide shell crystallites and between the Fe-oxide shell crystallites through the grain boundaries. Therefore, when the temperature is raised, the MR ratio is further reduced [Figs. 1(b) and 3(b)] because the magnetization of the shell crystallites is more highly disordered.

Finally, it is worth further discussing the effect of R_{O2} and d on the temperature and magnetic field dependence of the *MR* ratio (Figs. 5 and 6). In Fig. 5, the thinner the Fe-oxide shell layer (namely, the smaller the R_{O2}), the smaller is the absolute *MR* value at $T = 300$ K under the whole applied magnetic field range. At $T \leq 100$ K, however, the absolute *MR* value for the lowest R_{O2} is largest for $H \leq 10$ kOe, and then becomes smallest for $T > 35$ kOe. In Fig. 6, moreover, the larger the d, the larger is the *MR* value at low temperatures and low magnetic fields. Such R_{O2} and d dependent behaviors of the *MR* ratio can be understood by the exchange interaction between the FM Fe cores and spin-glass-like Fe-oxide shells, and by observing the virgin magnetization curves at different temperatures [Fig. 7(a)]. As seen in Fig. 7(a), with increasing H, the magnetization at high temperatures clearly increases more rapidly than that at low temperatures for $H \leq 10$ kOe because of the disappearance of the exchange interaction at high temperatures.[15] With increasing R_{O2} or decreasing d, the exchange interaction is enhanced due to the decrease of the volume fraction of the Fe core to Fe-oxide shell, so that the sample with the lowest R_{O2} or largest d reveals the largest *MR* value at low temperatures and low magnetic fields.

5. Conclusions

The transport properties and *MR* effects in the size-monodispersed oxide-coated Fe cluster assemblies with the mean cluster sizes of 9–17 nm have been investigated, and their dependence on the O_2 gas flow ratio R_{O2}, mean cluster size d, temperature, and magnetic field have been discussed. For the pure Fe cluster assembly, an ordinary metallic temperature dependence and a small positive *MR* effect up to $H = 50$ kOe were observed. For the oxide-coated Fe cluster assemblies ($R_{O2} \geq 0.2$ sccm), the temperature coefficient of the resistivity (TCR) becomes negative and the two-step-type linear $\log\rho$–$1/T$ temperature dependence of the resistivity at low and high temperatures was observed, similar to the size-monodispersed CoO-coated Co cluster assemblies,[17] mainly originating from the tunnel-type conduction between the cluster cores through the oxide shell layers at low temperatures, and the thermal-activated-type conduction in the nonstoichiometric semiconductor oxide shell layers at high temperatures. The oxide-coated Fe cluster assemblies exhibit a large negative *MR* effect which is further enhanced at low temperatures due to the dominant contribution of the spin-dependent tunneling process between the Fe cores. It has been found that the magnetic field dependence of the *MR* ratio at all temperatures shows no saturation tendency and completely disagrees with the magnetization curves which gives the saturation tendency in spite of a gradual increase of magnetization for $H > 10$ kOe, being different from the CoO-coated Co cluster assemblies where the magnetic field dependence of the *MR* ratio is well correlated with the magnetization curve and exhibits saturation behavior. Such a high-field nonsaturation feature in *MR* can be attributed to the spin-disordered structure, which was frozen in a spin-glass-like state at low temperatures, of the surface of the Fe-oxide shell crystallites or the whole thinner Fe-oxide shell layers.

Acknowledgments

This work was supported by Core Research for Evolutional Science and Technology (CREST) of Japan Science and Technology Corporation (JST), a Grant-in-aid for Scientific Research supported by the Ministry of Education, Culture, Sports, Science and Technology, and a Grant-in-aid for Intellectual Cluster Project supported by the Ministry of Education, Culture, Sports, Science and Technology, Aichi Prefecture and Aichi Science and Technology Foundation. One of the authors (D. L. Peng) acknowledges the financial support from the Japan Society for the Promotion of Science (JSPS). We appreciate the help of Mr. T. Asai and N. Nozawa with the sample preparation.

1) *Nanomaterials: Synthesis, properties and Applications*, eds. A. S. Edelstein and R. C. Cammarata (Institute of Physics, Bristol, 1996).
2) P. Sheng, B. Abeles and Y. Arie: Phys. Rev. Lett. **31** (1973) 44.
3) J. S. Helman and B. Abeles: Phys. Rev. Lett. **37** (1976) 1429.
4) S. Maekawa and Gäfvert: IEEE Trans. Magn. **18** (1982) 707.
5) J. C. Slonczewski: Phys. Rev. B **39** (1989) 6995.
6) B. Dieny, V. S. Speriosu, S. S. P. Parkin, B. A. Gurney, D. R. Wilhoit and D. Mauri: Phys. Rev. B **43** (1991) 1297.
7) A. Hernando: J. Phys.: Condens. Matter **11** (1999) 9455.
8) W. H. Meiklejohn and C. P. Bean: Phys. Rev. **102** (1956) 1413.
9) W. H. Meiklejohn and C. P. Bean: Phys. Rev. **105** (1957) 904.
10) S. Gangopadhyay, G. C. Hadjipanayis, C. M. Sorensen and K. J. Klabunde: Nanostruct. Mater. **1** (1992) 449.
11) S. Gangopadhyay, G. C. Hadjipanayis, C. M. Sorensen and K. J. Klabunde: J. Appl. Phys. **73** (1993) 6964.
12) S. Gangopadhyay, G. C. Hadjipanayis, B. Dale, C. M. Sorensen, K. J. Klabunde, V. Papaefthymiou and A. Kostikas: Phys. Rev. B **45** (1992) 9778.
13) L. Del Bianco, A. Hernando, M. Multigner, C. Prados, J. C. Sanchez-Lopez, A. Fernandez, C. F. Conde and A. Conde: J. Appl. Phys. **84** (1998) 2189.
14) D. L. Peng, K. Sumiyama, T. Hihara, S. Yamamuro and T. J. Konno: Phys. Rev. B **61** (2000) 3103.
15) D. L. Peng, T. Hihara, K. Sumiyama and H. Morikawa: J. Appl. Phys. **92** (2002) 3075.
16) L. Del Bianco, D. Fiorani, A. M. Testa, E. Bonetti, L. Savini and S. Signoretti: Phys. Rev. B **66** (2002) 174418.
17) D. L. Peng, K. Sumiyama, T. J. Konno, T. Hihara and S. Yamamuro: Phys. Rev. B **60** (1999) 2093.
18) S. Yamamuro, K. Sumiyama, M. Sakurai and K. Suzuki: Supramol. Sci. **5** (1998) 239.
19) D. L. Peng, K. Sumiyama, T. Hihara and T. J. Konno: Scripta Mater. **44** (2001) 1471.
20) H. Sato, I. Sakamoto and C. Fierz: J. Phys.: Condens. Matter **3** (1991) 9067.
21) C. Uher, R. Clarke, G. Zheng and I. K. Schuller: Phys. Rev. B **30** (1984) 453.
22) M. T. Perez and J. L. Vicent: Phys. Rev. B **38** (1988) 9503.

23) A. Carl, G. Dumpich and D. Hallfarth: Phys. Rev. B **39** (1989) 915.
24) A. Carl, G. Dumpich and D. Hallfarth: Phys. Rev. B **39** (1989) 3015.
25) A. Carl, G. Dumpich and D. Hallfarth: Thin Solid Films **193/194** (1990) 1065.
26) B. Abeles, Ping Sheng, M. D. Coutts and Y. Arie: Adv. Phys. **24** (1975) 407.
27) J. S. Helman and B. Abeles: Phys. Rev. Lett. **37** (1976) 1429.
28) J. Inoue and S. Maekawa: Phys. Rev. B **53** (1996) R11927.
29) C. L. Chien, J. Q. Xiao and J. S. Jiang: J. Appl. Phys. **73** (1993) 5309.
30) S. Gangopadhyay, G. C. Hadjipanayis, B. Dale, C. M. Sorensen and K. J. Klabunde: Nanostruct. Mater. **1** (1992) 77.
31) K. Haneda and A. H. Morrish: Surf. Sci. **77** (1978) 584.
32) S. Linderoth, S. Morup and M. D. Bentzon: J. Mater. Sci. **30** (1995) 3142.
33) L. Bel Bianco, A. Hernando, E. Bonetti and E. Navarro: Phys. Rev. B **56** (1997) 8894.
34) R. H. Kodama, A. E. Berkowitz, E. J. McNiff and S. Foner: Phys. Rev. Lett. **77** (1996) 394.
35) R. H. Kodama and A. S. Edelstein: J. Appl. Phys. **85** (1999) 4316.
36) B. Martinez, X. Obradors, Ll. Balcells, A. Rouanet and C. Monty: Phys. Rev. Lett. **80** (1998) 181.
37) E. Tronc, A. Ezzir, R. Cherkaoui, C. Chanéac, M. Noguès, H. Kachkachi, D. Fiorani, A. M. Testa, J. M. Grenèche and J. P. Jolivet: J. Magn. Magn. Mater. **221** (2000) 63.